**Atmospheric
Chemistry
and Physics
Discussions**

Sulfur isotope fractionation during oxidation of sulfur dioxide: gas-phase oxidation by OH radicals and aqueous oxidation by H_2O_2, O_3 and iron catalysis

E. Harris[1], B. Sinha[1], P. Hoppe[1], J. N. Crowley[2], S. Ono[3], and S. Foley[4]

[1]Abteilung Partikelchemie, Max-Planck-Institut für Chemie, Becherweg 27, 55128 Mainz, Germany
[2]Abteilung Luftchemie, Max-Planck-Institut für Chemie, Becherweg 27, 55128 Mainz, Germany
[3]Department of Earth, Atmospheric, and Planetary Sciences, Massachusetts Institute of Technology, 77 Massachusetts Avenue, Cambridge, MA 02139, USA
[4]Earth System Science Research Centre, Institute for Geosciences, University of Mainz, Becherweg 21, 55128 Mainz, Germany

Correspondence to: B. Sinha (baerbel.sinha@mpic.de)

Discussion Paper | **Discussion Paper** | **Discussion Paper** | **Discussion Paper**

ACPD

11, 23959–24002, 2011

Sulfur isotope fractionation during oxidation of sulfur dioxide

E. Harris et al.

Title Page

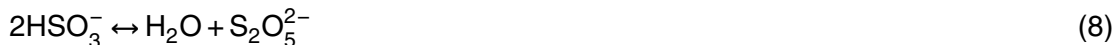| Abstract | Introduction |
| Conclusions | References |
| Tables | Figures |

|◄ | ►|

◄ | ►

Back | Close

Full Screen / Esc

Printer-friendly Version

Interactive Discussion

Abstract

The oxidation of SO_2 to sulfate is a key reaction in determining the role of sulfate in the environment through its effect on aerosol size distribution and composition. Sulfur isotope analysis has been used to investigate sources and chemistry of sulfur dioxide and sulfate in the atmosphere, however interpretation of measured sulfur isotope ratios is challenging due to a lack of reliable information on the isotopic fractionation involved in major transformation pathways. This paper presents measurements of the fractionation factors for the major atmospheric oxidation reactions for SO_2: Gas-phase oxidation by OH radicals, and aqueous oxidation by H_2O_2, O_3 and a radical chain reaction initiated by iron. The measured fractionation factor for $^{34}S/^{32}S$ during the gas-phase reaction is $\alpha_{OH} = (1.0089 \pm 0.0007) - ((4 \pm 5) \times 10^{-5}) T (^{\circ}C)$. The measured fractionation factor for $^{34}S/^{32}S$ during aqueous oxidation by H_2O_2 or O_3 is $\alpha_{aq} = (1.0167 \pm 0.0019) - ((8.7 \pm 3.5) \times 10^{-5}) T (^{\circ}C)$. The observed fractionation during oxidation by H_2O_2 and O_3 appeared to be controlled primarily by protonation and acid-base equilbria of S(IV) in solution, and there was no significant difference between the fractionation produced by the two oxidants within the experimental error. The isotopic fractionation factor from a radical chain reaction in solution catalysed by iron is $\alpha_{Fe} = (0.989 \pm 0.0043)$ at $19\,^{\circ}C$ for $^{34}S/^{32}S$. Fractionation was mass-dependent with regards to ^{33}S for all the reactions investigated. The radical chain reaction mechanism was the only measured reaction that had a faster rate for the light isotopes, and will be particularly useful to determine the importance of the transition-metal catalysed oxidation pathway.

1 Introduction

Sulfate and sulfur dioxide play an important role in environmental chemistry and climate through their effect on aerosols. The majority of anthropogenic sulfur is released directly as SO_2, and a significant fraction of biogenic and natural sulfur (e.g. OCS,

DMS) is also either directly released as SO_2 or oxidised to SO_2 in the atmosphere (Berresheim et al., 2002; Seinfeld and Pandis, 1998). Around 50 % of global atmospheric sulfur dioxide is then oxidised to sulfate, while the rest is lost through dry and wet deposition (Chin et al., 1996). The oxidation pathway – heterogeneous or homogeneous – is an important factor because it determines the effect that sulfate will have on the environment.

Homogeneous oxidation in the gas phase by OH radicals follows several steps (Tanaka et al., 1994):

$$SO_2 + OH + M \rightarrow HOSO_2 + M \tag{1}$$

$$HOSO_2 + O_2 \rightarrow SO_3 + HO_2 \tag{2}$$

$$SO_3 + H_2O \rightarrow H_2SO_4 \tag{3}$$

The product is sulfuric acid gas, which can stick to the surface of existing particles or nucleate to form new particles in the atmosphere (Benson et al., 2008; Kulmala et al., 2004). These new particles have a direct radiative effect and may also grow to act as cloud condensation nuclei (CCN).

Heterogeneous oxidation acts upon S(IV) in solution or on particle surfaces. The major oxidants are H_2O_2 and O_3, and transition metals such as Fe^{2+}/Fe^{3+}, which catalyse a radical chain reaction pathway where O_2 acts as the oxidant (Herrmann et al., 2000). The dissolution of SO_2 before oxidation follows several steps (Eriksen, 1972a):

$$SO_2(g) \leftrightarrow SO_2(aq) \tag{4}$$

$$SO_2(aq) + H_2O \leftrightarrow HSO_3^- + H^+ \tag{5}$$

$$HSO_3^- + H^+ \leftrightarrow H_2SO_3 \tag{6}$$

$$HSO_3^- \leftrightarrow SO_3^{2-} + H^+ \tag{7}$$

$$2HSO_3^- \leftrightarrow H_2O + S_2O_5^{2-} \tag{8}$$

Equation (6) has a pK_a of 1.77 and Eq. (7) has a pK_a of 7.19 (Moore et al., 2005). Oxidation by H_2O_2 is not significantly dependent on pH within normal atmospheric pH ranges (pH = 2–7), while oxidation by transition metal catalysis and O_3 becomes faster as pH increases (Seinfeld and Pandis, 1998). Heterogeneous oxidation produces sulfate on the surface of particles or in droplets, changing their CCN activity and lifetime through growth and increased hygroscopicity (Bower and Choularton, 1993; Mertes et al., 2005). Thus, a comprehensive knowledge of the oxidation and removal of SO_2 and sulfate is key to understanding and modelling aerosol and cloud formation and processes and their effects on past and future climate.

Aerosol direct and indirect effects continue to contribute the largest uncertainty to estimates of anthropogenic global mean radiative forcing (IPCC, 2007). Global emissions of anthropogenic sulfur in Europe and North America have decreased significantly in the past few decades, however as Asian sulfur emissions are increasing due to energy demand and coal use, and are not expected to decrease until at least 2020 (IPCC, 2007), anthropogenic emissions are likely to remain the major global source of non-sea salt sulfate (Chin et al., 1996; Seinfeld and Pandis, 1998). Understanding the sulfur cycle is therefore necessary to reduce the uncertainty in aerosol forcing estimates.

This study presents measurements of the stable isotope fractionation during gas-phase oxidation by the OH radical and oxidation in the aqueous phase with H_2O_2, O_3 and iron catalysis as terminating reactions. These reactions are considered to be the most important sulfur dioxide oxidation pathways on a global scale. We demonstrate that stable sulfur isotope ratios can be used to constrain atmospheric sulfur oxidation pathways and are particularly useful to quantify the importance of radical chain reactions for the atmospheric sulfur cycle.

2 Sulfur isotopes in the environment

The isotopic composition of sulfur in the environment reflects its sources, transport and chemistry, so measurements of stable sulfur isotopes can be effectively used to constrain the sulfur cycle. Sulfur has four naturally-occurring stable isotopes: ^{32}S, ^{33}S, ^{34}S and ^{36}S. The isotopic composition of a sulfur sample is represented by its delta value, which is the ratio of a heavy isotope to the most abundant isotope (^{32}S) in the sample compared to a standard ratio and expressed in permil:

$$\delta^x S\,(‰) = [\frac{(\frac{n(^xS)}{n(^{32}S)})_{sample}}{(\frac{n(^xS)}{n(^{32}S)})_{V-CDT}} - 1] \times 1000 \tag{9}$$

where ^{x}S is one of the heavy isotopes, ^{33}S, ^{34}S or ^{36}S, and V-CDT is the international sulfur isotope standard, Vienna Canyon Diablo Troilite, which has isotopic ratios of ^{34}S/^{32}S = 0.044163 and ^{33}S/^{32}S = 0.007877 (Ding et al., 2001).

Chemical reactions, for example the oxidation of SO_2 to sulfate, cause fractionation of isotope ratios between reactions and products as long as the reaction does not go to completion. The fractionation may be due to equilibrium or kinetic discrimination, and is represented by the fractionation factor α. For an irreversible reaction, fractionation is kinetic and alpha is the ratio of the rate constants: $\alpha = k_x/k_{32}$. Thus, $\alpha > 1$ indicates that the heavy isotopes react faster than the light isotopes. The permil differences between reactions and products with regards to α and reaction extent in a closed system are described by the Rayleigh laws (Mariotti et al., 1981; Krouse and Grinenko, 1991), which are discussed in Sect. 3.3.2. Thus, isotopic fractionation can not only distinguish between reactions: For known irreversible reactions in a closed system, the isotopic fractionation can provide quantitative information about how far the reaction has gone to completion.

The isotopic composition of many major sources of atmospheric sulfur have been measured (e.g., Novak et al., 2001a; Patris et al., 2000; Rees et al., 1978; Krouse and

Sulfur isotope fractionation during oxidation of sulfur dioxide

E. Harris et al.

E. Harris et al.

Grinenko, 1991), and the major limitation to interpreting atmospheric isotope measurements is the lack of laboratory studies of the isotopic fractionation factors involved in the most common atmospheric reactions of sulfur (Guo et al., 2010; Norman et al., 2006; Sinha et al., 2008a). For heterogeneous oxidation, equilibrium fractionation of $^{34}S/^{32}S$ during the uptake of SO_2 into solution and the subsequent acid-base equilibria has been measured in several studies. The results range between 1.010 and 1.017 at 25 °C (Egiazarov et al., 1971; Eriksen, 1972a). So far, the isotopic effect of the terminating oxidation of S(IV) to S(VI) has not been investigated.

The kinetic fractionation during gas-phase oxidation of SO_2 by OH radicals has been estimated to be $\alpha = 0.991$ by ab initio calculations (Tanaka et al., 1994) or to be $\alpha = 1.14$ by RRKM theory (Leung et al., 2001). The discrepancy between these two estimates is larger than the measured variation in atmospheric sulfur samples (Norman et al., 2006). Several atmospheric studies have also tried to infer the fractionation during this reaction. Seasonality in data, with lower $\delta^{34}S$ values measured in summer, could show that the gas-phase fractionation factor is less than the heterogeneous fractionation factor and probably less than 1 (Saltzman et al., 1983; Sinha et al., 2008a). However, seasonality may also be explained by changing sources or the temperature-dependence of fractionation factors (Caron et al., 1986; Novak et al., 2001a; Ohizumi et al., 1997). The study of $\Delta^{17}O$ of sulfate trapped in ice cores showed that the ratio of gas-phase to aqueous-phase oxidation was higher and the $\delta^{34}S$ was lower during the last glacial maximum than the preceeding and subsequent interglacials (Alexander et al., 2002, 2003). The authors suggest isotopic fractionation progressively affects the SO_2 reservoir during transport as the sulfate is removed quickly, thus the data would show that $\alpha_{hom} > \alpha_{het}$. However, this progressive depletion in the reservoir signature has not been explicitly modelled and compared with measurements, so the isotopic composition in the ice-core could be directly representative of the oxidation and show that $\alpha_{hom} < \alpha_{het}$. Therefore, the goal of this study is to determine sulfur isotope fractionation factors for the main oxidation pathways of SO_2 to facilitate the use of sulfur isotopes in understanding the atmospheric sulfur cycle.

3 Experimental

3.1 Apparatus

The reaction system used to investigate the oxidation of SO_2 is shown in Fig. 1. The reactors were made of glass and their internal surfaces were coated with FEP 121a (Dupont) to minimise wall loss of H_2SO_4. PFA tubing and connectors were used for gas transfer between experimental components. Pressure was monitored with a capacitance manometer. The reactor had a thermostatted jacket connected to a circulating cooler (Julabo Labortechnik GmbH, Model F81-HL) to regulate temperature. The actual gas-phase reaction temperature was calibrated to the set temperature of the Julabo instrument with a PT-100 Ω resistance sensor fitted into the glass reactor. The flows of all gases to the reactor were controlled using mass flow controllers referenced to standard conditions of temperature and pressure for N_2 ($T_s = 273.15$ K, $P_s = 1013.25$ mBar) (MKS Instruments Deutschland GmbH, uncertainty = 0.5 % of reading plus 0.2 % of full scale), and flows and leaks were checked regularly with a Gilibrator (Sensidyne, uncertainty < 1 % of reading). SO_2 gas (Westfalen AG, Linde AG, both 102 ppm±2 % in synthetic air) was diluted with synthetic air (Westfalen AG, 20.5 % O_2 in N_2) to the desired concentration before it entered the reactor. The outflow from the reactor passed through the H_2SO_4 glass and SO_2 bubbler collectors, described in detail in Sect. 3.3. Most experiments were run for 7–8 h to generate sufficient product for isotopic analysis. The exact conditions of each experiment are detailed in the relevant section.

Following each experiment, the collection systems were emptied immediately. The solution from the SO_2 bubblers, containing hydrogen peroxide and sulfate, was poured into a clean beaker and the bubblers were rinsed with MilliQ water several times into the beaker. The H_2SO_4 trap was rinsed at least five times with MilliQ water to remove all the adsorbed H_2SO_4, and the solution was collected in a beaker. An excess of $BaCl_2$ was added to each solution to precipitate S(VI) as $BaSO_4$, as well as sufficient HCl to lower the pH to approximately 3 for optimal precipitation (Rees and Holt, 1991). After at least 12 h to ensure complete precipitation, the solutions were filtered through gold-

coated Nucleopore filters with 0.2 µm pores. Several rinses with MilliQ water removed any remaining $BaCl_2$ from the $BaSO_4$ precipitate and the filters were dried at room temperature. Samples with a large amount of material, where sulfate grains were clumped in groups, were gold-coated to prevent charging during SEM and NanoSIMS analysis.

3.2 SEM and NanoSIMS analysis

3.2.1 Scanning electron microscopy

A LEO 1530 field emission scanning electron microscope (SEM) with an Oxford Instruments ultra-thin-window energy-dispersive x-ray detector (EDX) was used to locate and characterise particles before NanoSIMS analysis. The samples were directly analysed in the SEM after collection on gold-coated filters without any further treatment. The SEM was operated with an accelerating voltage of between 10 and 20 keV, a 60 µm aperture and a working distance of 9.6 mm. "High current mode" was used to increase the EDX signal and improve elemental sensitivity. All samples were viewed with the SEM to investigate the coverage, size and shape of sulfate grains. A transfer of the coordinate system between the NanoSIMS and the SEM is possible using several well-defined origin points, which allows the same grain or area to be found and analysed in both instruments. An example of a barium sulfate grain with its EDX spectrum is shown in Fig. 2.

3.2.2 Quantification with the SEM

The EDX spectrum can be used to roughly quantify compounds and particles on the filters, and thus estimate the extent of reactions. An automatic analysis of the filter is taken, with EDX analysis points distributed at regular intervals in each image. As long as the diameter of the largest particle is smaller than the distance between EDX points, the probability of the point falling on a particular particle is proportional to the

area covered by that type of particle (Winterholler, 2007). Moreover, if an element is just in one form, for example sulfur is only present as $BaSO_4$, the number of points with a sulfur signal will be proportional to the area covered by $BaSO_4$. The volume and hence mass of $BaSO_4$ can be found by considering the average height of the $BaSO_4$ grains, as long as it is evenly distributed and not clumped in large heaps. The sample height was estimated to be $0.2\,\mu m$ based on the movement in the Z-direction of the microscope needed to focus on the filter and on the top of a representative number of $BaSO_4$ grains. The largest source of uncertainty for quantification of the collected $BaSO_4$ is that grains can flake of the filter during handling of the samples.

The presence of a "signal" for an element in this quantification method requires differentiating between background noise and actual signal. Quantifying sulfur compounds on gold filters is challenging, because the gold peak overlaps strongly with the sulfur peak, as shown in Fig. 2. The contribution of the gold peak to the sulfur peak approximately follows a Gaussian distribution, as gold is present in all sampled EDX points. An example is shown in Fig. 3. The sulfur signal is superimposed on the Gaussian distribution of the gold signal, as the X-ray emission depth and spot size means the gold signal will always be present even when the sampling point falls on a barium sulfate grain (Goldstein et al., 1981). Thus, the presence of a significant sulfur signal was defined as falling above the 99.9 % confidence limit for the gold Gaussian distribution ($x > \mu + 3.09\sigma$). The contribution of S in $BaSO_4$ to the signal in the sulfur channel shows a peak, however the number of sulfur points is too low to calculate the Gaussian distribution for these samples. To account for the tail of the Gaussian curve of Au that is above the 3.09σ limit, which could be a large part of the signal at low sulfate concentrations, the integrated background above the 3.09σ limit was subtracted, and the number of points with a significant sulfur signal was defined as:

$$n(x > \text{bcg}) = n(x > \mu + 3.09\sigma) - 0.001[n(\text{total})] \tag{10}$$

The Gaussian curve does not always fit cleanly to the data. For samples where the area coverage is significantly less than 25 %, a second estimate of the 3σ limit can be approximated by $Q_u + 1.726(Q_u - Q_l)$, where Q_u and Q_l are the upper and lower

quartiles of the raw signal for the element of interest. This has previously been used to define the background of an SEM-EDX signal for a similar quantification method (Winterholler, 2007; Stoyan, 1998). EDX points with the signal for both barium and sulfur above the background are then used to quantify $BaSO_4$. The quantity of sulfate measured for a sample with the two methods has an average difference of 40 % and shows no systematic offset. The sulfate production in each experiment is an average of at least two duplicate samples both measured with the two methods. The limit of detection for quantification is the amount of sulfate when only one point shows a significant signal, and thus it depends on the total number of points taken. For most samples 10 000 EDX points were measured, giving a detection limit of 0.2 nmol of sulfate, or 0.18 ppb at the typical flow rate of 600 sccm.

3.2.3 NanoSIMS

The sulfur isotopic composition was determined with the Cameca NanoSIMS 50 ion probe at the Max Planck Institute for Chemistry in Mainz (Hoppe, 2006; Groener and Hoppe, 2006). The NanoSIMS 50 has a high lateral resolution (<100 nm) and high sensitivity and can simultaneously measure up to five different masses through a multicollection system, allowing high precision analysis of the small sample quantities required for this study. The use of this instrument to analyse sulfur isotope ratios is described in detail elsewhere (Winterholler et al., 2006, 2008), and only a brief description will be given here.

$BaSO_4$ is analysed directly without further processing after it is collected on gold-coated filters as described in Sect. 3.1. A $\sim$1 pA Cs^+ beam is focussed onto a $\sim$100 nm sized spot and rastered in a 2 µm×2 µm grid over the grain of interest. The ejected secondary ions are carried into the mass spectrometer and multicollection system. Each measurement consists of 200–400 cycles of 4.096 s duration preceded by varying lengths of presputtering until the gold coating is removed and the count rate is stable. Presputtering is carried out on an area of at least 10 µm×10 µm to avoid crater effects in the analysed area. Secondary ions of $^{16}O^-$, $^{32}S^-$, $^{33}S^-$, $^{34}S^-$ and $^{36}S^-$ were simul-

taneously detected in five electron multipliers at high mass resolution (M/ΔM >3900 for [33]S). The detector dead time is 44 ns and the count rates were corrected accordingly. The energy slit was set at a bandpass of 20 eV and the transmission was set at 15–20 % with the fifth entrance slit (10 × 100 µm) and the fourth aperture slit (80×80 µm) in
5 order to reduce the effect of quasi-simultaneous arrival (QSA; Slodzian et al. (2001)).

Mass-dependent and mass-independent instrumental mass fractionation (IMF) can occur at several stages of the SIMS analysis, so the IMF correction factor in each measurement session is determined with the commercially available $BaSO_4$ isotope standards IAEA-SO5 and IAEA-SO6. Correction for the quasi-simultaneous arrival
10 (QSA) effect was carried out as described by Slodzian et al. (2004), however a factor of 0.75 rather than 0.69 was used as this minimised the dependence on count rate best for these samples.

The number of counts is assumed to follow a Poisson distribution, so the counting statistical error is $\sqrt{n}$, i.e. the relative error is $1/\sqrt{n}$ (Bevington and Robinson, 1992).
15 Some spot-to-spot variation is also seen between individual measurements on a filter, most likely due to topographic effects or nanoscale inhomogeneity. Thus, at least five grains on each sample filter were measured, and a weighted average was calculated using $1/\sigma^2$ for the weighting function, where σ is the counting statistical error of individual measurements. To calculate the overall measurement uncertainty the error of
20 the weighted mean is multiplied by $\sqrt{\chi^2}$ for $\chi^2 >1$ in order to account for the larger uncertainty introduced by the spot-to-spot variability. The counting statistical error was typically 1–2 ‰ and the overall error for each sample 2–5 ‰.

3.3   Collection of SO_2 and H_2SO_4 products

3.3.1 H_2SO_4 collection

25 Sulfuric acid gas (in gas-phase oxidation experiments) and sulfate in aqueous droplets (for aqueous oxidation experiments) are first removed from the product gas stream by irreversible "wall loss" in a glass vessel with high surface area (Fig. 1). Particles are lost

by diffusion and electrostatic attraction leading to collisions with the walls (Lai, 2006). This is a bulk process and is assumed not to introduce a significant isotopic effect.

The loss of $H_2SO_4(g)$ to the walls of glass vessels is described by (Hanson and Eisele, 2000; Young et al., 2008):

$$[H_2SO_4]_t = [H_2SO_4]_0 e^{-kt} \tag{11}$$

where $[H_2SO_4]_0$ and $[H_2SO_4]_t$ are the gas phase concentration of H_2SO_4 at time = 0 and time $= t$, k is the diffusion-limited first order reaction coefficient: $k = 3.65\frac{D}{r^2}$, D is the diffusion coefficient and r is the radius of the reactor (Zasypkin et al., 1997). $D = 0.095\,\text{cm}^2\,\text{s}^{-1}$ in dry air at atmospheric pressure and decreases to $0.075\,\text{cm}^2\,\text{s}^{-1}$ at high humidity (Hanson and Eisele, 2000). These equations apply only to well-established laminar flow conditions in a cylindrical reactor and can just provide an estimate to wall loss in this system. Actual wall loss will be higher than predicted as turbulence in the system will increase the frequency of collisions with the walls.

Equation 11 can be rearranged to show the percentage of H_2SO_4 lost:

$$\%\,\text{lost} = \left(1 - \frac{[H_2SO_4]_t}{[H_2SO_4]_0}\right) \times 100 = (1 - e^{-kt}) \times 100 \tag{12}$$

At typical reaction conditions of 50 % humidity and 1000 sccm flow in a collector with a diameter of 4 cm, a total length of 70 cm is required to capture 99 % of the H_2SO_4 on the walls. The internal surface area will be increased by adding roughness to the glass walls so this is a minimum value of the predicted efficiency of the collectors shown in Fig. 1. At this efficiency, there should be no significant difference between the initial and the product isotopic composition.

No isotopic standard of gaseous H_2SO_4 was available, so the fractionation during collection was measured by analysing the product from two collectors arranged in series. A flow of N_2 *6.0* (Westfalen AG) was passed through a 1 M solution of H_2SO_4 and the resulting mixture flowed through the two 40 cm long glass collection vessels. Following the experiment, the sulfate was precipitated and analysed as described in

Sect. 3.1 and 3.2 respectively. The average measured differences between the δ^{34}S and δ^{33}S of the two collectors are -1.1 ± 2.6 ‰ and -0.3 ± 1.5 ‰ respectively, showing that there is no systematic fractionation introduced beyond the precision of the measurement (Table 1). A small or insignificant difference between the two collectors can only be achieved with a low collection efficiency or a fractionation factor close to 1, otherwise the δ^{34}S and δ^{33}S of the H_2SO_4 entering the second collector would be altered by the first collector. A high efficiency was theoretically predicted, and supported by the fact that very little product was seen on the second filter during analysis. Therefore, the fractionation introduced by this collection method is insignificant and the δ^{33}S and δ^{34}S of H_2SO_4 in later experiments does not need to be corrected for an isotopic change during collection.

It is important to consider possible breakthrough of H_2SO_4 gas to the SO_2 gas collection system. Although H_2SO_4 is efficiently removed, when the H_2SO_4 concentration was more than three times as high as the SO_2 concentration, breakthrough of H_2SO_4 could be detected in the isotopic composition of SO_2. The sensitivity to breakthrough also depends on the difference in δ^{34}S between SO_2 and H_2SO_4. To completely avoid effects from breakthrough of H_2SO_4, the concentration of SO_2 was kept at least twice as high as the concentration of H_2SO_4, i.e. the reaction yield was kept below one third of the total SO_2.

3.3.2 SO_2 collection

Sulfur dioxide is traditionally collected on filters impregnated with alkaline solutions such as Na_2CO_3 (Novak et al., 2001a; Huygen, 1963). A variety of solutions were tested with varying amounts of Na_2CO_3, $BaCl_2$, triethanolamine, glycerol and H_2O_2, and the average fractionation factor was measured as $\alpha = 1.007\pm0.003$ for all methods tested. The recovery of SO_2 was found to vary from less than 5 % to more than 40 % depending on the length of time that SO_2 was collected and the amount taken up relative to the alkalinity capacity of the filter, rather than on the solution composition.

The fractionation in the final product could then vary from at least 4.5 to 10.6‰, with even larger variations introduced for longer experiments or very high filter loads. This method of collection is not suitable for our laboratory experiments due to the low relative humidity and high concentrations of SO_2 in our samples combined with the need for a constant, correctable isotopic fractionation.

Alternatively, SO_2 can be collected by passing the gas stream through bubblers containing hydrogen peroxide, which oxidises the S(IV) in the solution to sulfate (US-EPA, 2010). This method was tested by passing SO_2 of known isotopic composition ($\delta^{34}S$ = 1.25±0.3‰) through two bubblers in series containing a solution of hydrogen peroxide, held at 0°C in an ice bath to increase SO_2 solubility (Fig. 1). Following the experiment a $BaSO_4$ precipitate was prepared and analysed as described in Sects. 3.1 and 3.2. This experiment was repeated eight times, of which seven were analysed as described in Sect. 3.2.3. One sample was analysed by traditional dual-inlet isotope ratio mass spectrometry at the Massachusetts Institute of Technology according to the methods described in Ono et al. (2006a). The reaction conditions and results are shown in Table 2 and Fig. 4.

The isotopic composition of the product depends on the value of the kinetic fractionation factor α ($= k_{34}/k_{32}$) and the fraction of reactant remaining, as described by the Rayleigh fractionation laws (Mariotti et al., 1981; Nriagu et al., 1991):

$$\alpha = \frac{\ln\left[1 - (1-f)\frac{R_P}{R_0}\right]}{\ln(f)} \tag{13}$$

This can be used directly for the first bubbler, and adapted to represent the second bubblers in series:

$$\alpha_2 = \frac{\ln\left[1 - (1-f)\frac{R_{P_2}}{R_0^*}\right]}{\ln(f)} \tag{14}$$

where f is the fraction of reactant (SO_2) remaining and R_0, R_P and R_{P_2} are the isotope ratios $^{34}S/^{32}S$ for the initial gas, the product of the first and the product of the second

bubbler respectively. R_0^* is the initial isotopic composition entering the second bubbler, that is, the residual SO_2 remaining after the first bubbler: $R_0^* = R_0 f^{\alpha_1 - 1}$.

The collection efficiency $(1 - f)$ must be known to find α from these equations. Grains can flake off the filter during handling when a large amount of product is present, lead-
5 ing to greater losses from the filter from the first bubbler as it has more product. Thus quantification by SEM-EDX as described in Sect. 3.2.1 does not give an accurate value for f. Gravimetric determination of f is not possible due to the very small quantities of sulfate and the interference from coprecipitated $BaCl_2$. The fraction of SO_2 remaining was therefore determined as the value that would give an equal α for the first and
10 second collectors, found for each experiment by iteration with Eq. (13) and (14). The weighted average of the individual values shows that 39 % of SO_2 is collected per bubbler. The total collection efficiency of two bubblers in series is 63 ±11 %.

Equations (13) and (14) were then used to find α for each bubbler measurement. The weighted average α_{34} is 1.016±0.0013, which results in a product $\delta^{34}S$ change of
15 +9.2±0.7‰ following the two bubblers. This is consistent with expectations for aque- ous oxidation by H_2O_2 (Eriksen, 1972a; Egiazarov et al., 1971) and is robust over a large range of flows and SO_2 concentrations. The gas temperature does not affect the measured fractionation since the collector is held at 0°C and the quantity of gas passed through the sampling system is not sufficient to change the temperature within
20 the collection system.

Measurements of $\delta^{33}S$ by NanoSIMS are more uncertain than $\delta^{34}S$ due to counting statistics. The measured α_{33} is 1.007±0.002, which is not significantly different from the value expected for mass-dependent fractionation (MDF = 0.515, t-test, $P = 0.05$). The mass-dependent nature of the fractionation is confirmed by the high precision
25 fluorination measurement of Sample 8, which showed $\Delta^{33}S = 0.05$ ‰. The change in $\delta^{34}S_{SO_2}$ and $\delta^{33}S_{SO_2}$ due to reactions of interest in subsequent experiments can be isolated by considering the measured fractionation due to collection and the initial isotopic composition.

3.4 Aqueous oxidation

3.4.1 Aqueous oxidation by the radical chain reaction mechanism

Aqueous oxidation by a radical chain reaction initiated by Fe^{3+} (see Herrmann et al. (2000)) was measured by bubbling SO_2 through a solution containing 0.1 M $Fe(Cl)_2$ and 0.1 M $Fe(Cl)_3$. The product sulfate was collected from two bubblers in series. The quantity and isotopic composition of the sulfate in the second bubbler was equal to that in the first bubbler, showing the SO_2 was not significantly depleted.

3.4.2 Aqueous oxidation by H_2O_2 and O_3

The fractionation during collection of SO_2 is a direct measure of the fractionation during oxidation of SO_2 by H_2O_2 in solution at 0 ˚C under non-equilibrium conditions. This reaction was run eight times, as described in Sect. 3.3.2.

Reactor 2 (Fig. 1) was run with high humidity to investigate aqueous oxidation by H_2O_2 and O_3 in droplets rather than a bulk solution. Although oxidation by ozone would initially dominate, the pH in the system would very quickly decrease as sulfate was generated so the bulk of the reaction would be due to H_2O_2 (Seinfeld and Pandis, 1998). The experiments were run at room temperature, and humid air was added both through the photolysis tube and through a second entry into the reactor normally used to monitor pressure. Neither flow passed through a trap to break up or remove large droplets, so they contained saturated air with droplets present. A very large amount of product was generated, which significantly altered the isotopic composition of the SO_2 gas. The fractionation factor α must therefore be found from the Rayleigh equations. The reaction extent can be found from the isotopic mass balance:

$$\delta^{34}S_i = f\delta^{34}S_{SO_2} + (1-f)\delta^{34}S_{H_2SO_4} \tag{15}$$

where $\delta^{34}S_i$ is the initial composition of SO_2 and $\delta^{34}S_{SO_2}$ and $\delta^{34}S_{H_2SO_4}$ are the isotopic compositions of residual SO_2 and product H_2SO_4 when a fraction f of the initial

SO_2 remains. Around 65 % of SO_2 was oxidised under high humidity conditions.

To isolate the effect of O_3 on the product isotopic composition, the reaction was run with a glass attachment that passed dry synthetic air over the Hg lamp to generate 1000 ppm ozone. As the photolysed air was dry the H_2O_2 concentration will be negligible. Humidified air at 40 % relative humidity was added to the reactor and was not exposed to UV light. The product sulfate and the residual SO_2 were collected and there was no significant change in the SO_2 isotopic composition.

3.5 Gas-phase oxidation

3.5.1 OH generation

OH was generated from the photolysis of water vapour at around 30 % relative humidity. 100 sccm of humidified nitrogen was passed over a low-pressure mercury vapour lamp (Jelight Company Inc., USA), which produces light at 184.9 nm resulting in the generation of OH radicals (Cantrell et al., 1997):

$$H_2O + h\nu \rightarrow OH + H \tag{16}$$

The OH concentration was determined from chemical titration of pyrrole (Sinha et al., 2008b, 2009), which entered the reactor through the SO_2 inlet and thus saw the same OH flux as SO_2. Two similar reactors were used to measure the OH + SO_2 reaction and the influence of potential interfering reactions (Fig. 1). Reactor 1 produced 11 ppb of OH. Reactor 2 did not produce detectable OH at the reaction point and was used to measure interferences. A small amount of OH would have been generated at the lamp tip, however the residence time of humidifed water at the lamp was short and all OH generated was lost before entering the reactor.

The OH concentration is dependent on the water vapour concentration (Young et al., 2008). In these experiments the relative humidity is kept constant by passing the humid air stream through glass wool held at the reaction temperature, in order to remove excess humidity and large droplets so that aqueous oxidation is minimised, thus the

water vapour concentration will change exponentially with temperature according to the vapour pressure of water. The quantity of sulfate produced at the four different reaction temperatures was measured as described in Sect. 3.2.2 and found to follow the expected exponential relationship as shown in Fig. 5.

3.5.2 Interferences

Possible interferences are sulfate impurities in reagents, direct photolysis of SO_2, and reaction in the gaseous or aqueous phase with oxidants such as H_2O_2, HO_2 and O_3, which are also generated during the photolysis of water (Atkinson et al., 2004). SO_2 photolysis can follow a number of pathways under UV light (Farquhar et al., 2001). The wavelength-dependent quantum yield of the different pathways is not well known and the fractionation occurring is not well-constrained (Farquhar et al., 2001; Lyons, 2009). The gas phase reactions of SO_2 with lamp products other than OH are very slow (Atkinson et al., 2004), however oxidation on glass surfaces with adsorbed water could lead to sulfate production.

The trace sulfate content present in the MilliQ water used to rinse the sulfate from the collectors was tested by adding $BaCl_2$ to 500 mL of MilliQ water. The $BaSO_4$ was then collected and quantified in the SEM. The interference from sulfate impurities in MilliQ water makes a contribution of 6 % of the total sulfate at −25 °C and is less than 2.5 % of sulfate for all other temperatures.

Direct photolysis was measured by running both Reactors 1 and 2 but adding humidity 10 cm after the lamp, to ensure the water was not photolysed while allowing Reaction 3 to occur. The rate of pyrrole photolysis was measured to be the same for both reactors, so it can be assumed that the photolysis of SO_2 is also comparable between the two reactors. Direct photolysis was measured with both the standard Hg lamp, which produces 185 and 254 nm lines, and with an O_3-free Hg lamp, which emits only the 254 nm line. Oxidation by lamp products other than OH, such as H_2O_2, HO_2 and O_3, was tested with Reactor 2, which passed water vapour through UV light but did not produce detectable OH, although concentrations of these secondary products

were likely to be lower in this reactor due to the shorter exposure time to the lamp. A facsimile model run of the species produced by Reactor 1 is shown in Fig. 6 for the photolysis of water in synthetic air to generate 11 ppb OH followed by immediate mixing with 1 ppm SO_2. The whole reaction system was also run with no lamps switched on to measure the quantity of sulfate oxidised by trace compounds in the water or glass walls. The quantification of these interferences is shown in Fig. 5. No sulfate was measured when SO_2 was run through the reaction system in the absence of humidity.

The quantity of sulfate collected in the absence of OH radicals was found to have an exponential relationship to temperature and thus was proportional to water vapour pressure. The measured temperature dependencies of sulfate quantity for no OH and OH experiments were adequately described by exponential curves and the fits were used to quantify the percentage contribution of the background to the total sulfate at each experimental temperature. The reaction of interest, SO_2 + OH, contributes between 77 and 85 % of the total collected sulfate, depending on the reaction temperature.

The quantity of sulfate produced under UV light does not significantly differ between Reactors 1 and 2, O_3-free or normal Hg lamps, and whether humidity is passed over the lamp or not. Thus, all experiments with UV light were combined to find a background of 0.60±0.40 ppb at room temperature. The quantity of sulfate produced in the absence of UV light was 1.04±0.10 ppb, i.e., compatible with the former value within errors, and the $\delta^{34}S$ values of the products are the same for all conditions (Fig. 7). As the average isotopic composition of the background ($\delta^{34}S = 13.0±1.5$ ‰) is consistent with that expected from aqueous oxidation ($\delta^{34}S = 15.1±0.4$ ‰), and the quantity of background sulfate varies with the vapour pressure of water, it can be assumed the background sulfate reaction is aqueous oxidation due to an impurity in the water or an oxidation reaction in an H_2O surface layer on the glass walls of the collector. As the fractionation for aqueous oxidation has a much lower uncertainty due to the large number of measurements and its temperature dependence is known, it can be used to correct for the background in the SO_2 + OH reaction.

4 Results and discussion

4.1 Aqueous oxidation

The fractionation factors during aqueous oxidation by H_2O_2, O_3 and radical chain re-
action initiated by Fe are shown in Fig. 8 and Table 3. All oxidants other than O_3
produce mass-dependent fractionation, and the deviation from the mass-dependent
fractionation line seen for O_3 may be a measurement artefact as only two samples
were measured. The radical chain reaction is the only measured aqueous reaction to
favour the light isotope. This agrees relatively well with measurements by Saltzman
et al. (1983), where a fractionation factor of 0.996 for oxidation of HSO_3^- by dissolved
O_2 was indicated by laboratory experiments.

4.1.1 Oxidation by H_2O_2 and O_3

The weighted linear fit to all points shown in Fig. 9 (except those for $SO_2(g) \leftrightarrow SO_2(aq)$)
shows that:

$$\alpha_{aq} = (1.0167 \pm 0.0019) - ((8.7 \pm 3.5) \times 10^{-5})T \tag{17}$$

where T is the temperature in degrees celsius. The temperature dependence is signifi-
cant at 99.9 % confidence. There is no significant difference between the α_{34} measured
for H_2O_2/O_3 and O_3 in droplets and the bulk H_2O_2 measurements, although the droplet
measurements have a much larger uncertainty. This is probably due to small variations
in humidity as well as the much smaller product quantities increasing the measurement
uncertainty.

Several previous studies have considered the fractionation during aqueous SO_2 ox-
idation and the combined results are presented in Fig. 9. Chmielewski et al. (2002)
and Eriksen (1972b) consider only the equilibrium $SO_2(g) \leftrightarrow SO_2(aq)$ and measure a
much lower fractionation factor ($\alpha = 1.00256$ at 18 °C). This shows that physical phase
transfer is responsible for only a small part of isotopic fractionation, and protonation

and acid-base equilibria in solution cause the majority of fractionation for the SO_2 (g) - S(IV) (aq) system.

The results of Egiazarov et al. (1971) and Eriksen (1972a,b,c,d) compare well with the results of the present study, although these earlier studies both consider only the equilibrium to S(IV) in solution while this study includes oxidation to S(VI). Eriksen (1972a) considers the equilibrium between $1\,M\,NaHSO_3$ at low pH as acid is constantly added to the system, thus the concentration of SO_3^{2-} will be negligible. The experiments of Egiazarov et al. (1971) consider the equilibration of $3\,M\,NaHSO_3$ at pH$\approx$4, so unlike Eriksen (1972a) these results will include some equilibration to SO_3^{2-} as well as significant production of $S_2O_5^{2-}$. The fractionation factor measured by Egiazarov et al. (1971) ($\alpha = 1.0173\pm0.0003$ at 25 °C) is slightly higher than the fractionation factor measured by Eriksen (1972a) ($\alpha = 1.01033\pm0.00041$ at 25 °C), suggesting that equilibration towards higher-pH forms of S(IV) introduces a further enrichment of ^{34}S. The rate of S(IV) oxidation by O_3 increases by several orders of magnitude as the pH increases above 5.5 (Botha et al., 1994), and the fractionation factor measured for O_3 in this study is slightly higher than that measured for H_2O_2 oxidation, supporting the hypothesis that equilibration to higher pH increases fractionation, while the terminating oxidation to O_3 may have little effect on isotopic fractionation. However, the difference between measured fractionation during oxidation by O_3 and H_2O_2 in this study is not significant considering the experimental error and a more detailed study of the pH-dependence of this system would be needed to fully resolve isotopic effects for each step in the pathway from $SO_2(g) \rightarrow$ sulfate.

4.2 Gas-phase oxidation of SO$_2$ by OH radicals

The oxidation of SO_2 by OH radicals in the gas phase was measured at four different temperatures in twelve individual experiments. The results are presented in Table 4 and Figure 10. The correction for aqueous background oxidation as described in Sect. 3.5.2 has only a small effect on the results as it accounts for less than 25 % of

sulfate production. The weighted fit to all points gives a temperature-dependent fractionation factor for ^{34}S of:

$$\alpha_{OH} = (1.0089 \pm 0.0007) - ((4 \pm 5) \times 10^{-5})T. \tag{18}$$

The measured fractionation factor for ^{33}S is

$$\alpha_{OH} = (1.0043 \pm 0.001) + ((1 \pm 4) \times 10^{-5})T. \tag{19}$$

This is not significantly different from the fractionation of ^{33}S predicted from a mass-dependent relationship to ^{34}S.

Ab initio calculations using transition state theory for the reaction SO_2 + OH → $HOSO_2$ by Tanaka et al. (1994) estimated a fractionation factor of 0.991, similar in magnitude but opposite in direction to the fractionation factor measured in this study. Leung et al. (2001) calculated the fractionation factor to be 1.14 based on RRKM theory. They found that although the positive difference in critical energies of the transition states would lead to a fractionation factor of < 1, this is overcome by the denser vibrational manifolds of the ^{34}S transition state. However, the authors state that even considering the uncertainties in all parameters used they predict a fractionation factor > 1.07, almost 10 times larger in magnitude than the factor measured in this study. Even a fractionation factor of 1.07 rather than 1.14 is significantly larger than the variation observed in atmospheric samples (e.g. Norman et al. (2006); Novak et al. (2001b)), so it is likely that RRKM theory can accurately predict only the direction and not the magnitude of this isotope effect.

4.3 Comparison to previous studies

A number of studies have used field measurements to estimate the value of the fractionation factors for SO_2 oxidation. Atmospheric measurements of $\delta^{34}S_{SO_4}$ and $(\delta^{34}S_{SO_4} - \delta^{34}S_{SO_2})$ are often lower in summer than in winter (Sinha et al., 2008a; Mukai et al., 2001; Saltzman et al., 1983). Oxidation by OH is expected to be highest in

summer and this may therefore show that the fractionation factor for gas-phase oxidation is lower than that for aqueous oxidation, in agreement with the results of this study. Observations that sometimes $\delta^{34}S_{SO_4} < \delta^{34}S_{SO_2}$ have previously been suggested to show that $\alpha_{OH} < 1$, however the results of this study point to a dominance of transition-metal catalysed oxidation for these samples. Seasonality is not a direct measurement of oxidation and fractionation but reflects changing sources and oxidation pathways as well as lifetime and removal mechanisms such as dry and wet deposition. Hence, in order to estimate fractionation factors from seasonal data, seasonal changes in oxidant concentrations, local sources and climatic conditions would need to be considered very carefully.

The $\delta^{34}S$ of stratospheric sulfate aerosol has been observed to first increase and then strongly decrease in the months following the eruption of Mt. Agung (Castleman et al., 1974), consistent with stratospheric oxidation favouring ^{34}S and progressively depleting the SO_2 reservoir. This was suggested to be consistent with oxidation by OH favouring the heavy isotope (Leung et al., 2001). However, strong $\Delta^{33}S$ signals found in ice core records of volcanic sulfate of the same event suggest photochemical oxidation is the dominant process producing these aerosols (Baroni et al., 2007, 2008), and they are thus not a good indicator of the magnitude and direction of α_{OH}.

Interglacial-glacial changes in $\Delta^{17}O$ of ice core sulfate can provide information on the oxidation pathways of sulfur due to the large $\Delta^{17}O$ signal in O_3 and the smaller but significant $\Delta^{17}O$ signal in H_2O_2 (Sofen et al., 2011; Alexander et al., 2002, 2003; Savarino et al., 2000). Transition metal-catalysed oxidation by O_2 and gas phase oxidation by OH both result in $\Delta^{17}O$ very close to 0 (Luz and Barkan, 2005; Sofen et al., 2011). The $\Delta^{17}O$ of ice core sulfate was larger in the surrounding interglacials than in the last glacial period, showing that oxidation by H_2O_2 and O_3 was proportionally more important in the interglacial periods. The $\delta^{34}S$ of sulfate was measured to be lower during glacial periods than surrounding interglacials (Alexander et al., 2003). It has been suggested that this shows a progressive depletion in ^{34}S during transport of SO_2 from lower latitude source regions, based on the α_{OH} of > 1.07 from Leung

et al. (2001). However, the results of this study suggest that the fractionation signature is directly transferred to ice-core sulfate, and increased oxidation by transition metal catalysis due to higher abundance of windblow dust could account for the lower values of δ^{34}S measured in glacial periods.

5   Conclusions

This study measured the fractionation factors for the most common pathways of SO_2 oxidation: gas phase oxidation by OH radicals, and aqueous phase oxidation by H_2O_2, O_3 and a radical chain reaction initiated by Fe. The fractionation factors for these oxidation pathways are now well constrained. This will allow stable sulfur isotopes to be used to understand the partitioning between these pathways in atmospheric samples. Modelling and field studies of sulfur isotopes in the atmosphere can use these fractionation factors to gain an increased understanding of the sulfur cycle and its effect on radiative forcing, aerosols and cloud condensation nuclei. Based on the unique fractionation factor of the reaction, sulfur isotope ratios will be particularly useful to constrain the importance of transition-metal catalysed sulfur oxidation in the atmosphere, which was the only reaction found to favour the light isotope in the current study.

References

Alexander, B., Savarino, J., Barkov, N. I., Delmas, R. J., and Thiemens, M. H.: Climate driven changes in the oxidation pathways of atmospheric sulfur, Geophys. Res. Lett., 29, 1685, doi:10.1029/2002GL014879, 2002. 23964, 23981

Alexander, B., Thiemens, M. H., Farquhar, J., Kaufman, A. J., Savarino, J., and Delmas, R. J.: East Antarctic ice core sulfur isotope measurements over a complete glacial-interglacial cycle, J. Geophys. Res.-Atmos., 108, 4786, doi:10.1029/2003JD003513, 2003. 23964, 23981

Atkinson, R., Baulch, D. L., Cox, R. A., Crowley, J. N., Hampson, R. F., Hynes, R. G., Jenkin, M. E., Rossi, M. J., and Troe, J.: Evaluated kinetic and photochemical data for atmospheric chemistry: Volume I - gas phase reactions of O_x, HO_x, NO_x and SO_x species, Atmos. Chem. Phys., 4, 1461–1738, doi:10.5194/acp-4-1461-2004, 2004. 23976

Baroni, M., Thiemens, M. H., Delmas, R. J., and Savarino, J.: Mass-independent sulfur isotopic compositions in stratospheric volcanic eruptions, Science, 315, 84–87, 2007. 23981

Baroni, M., Savarino, J., Cole-Dai, J. H., Rai, V. K., and Thiemens, M. H.: Anomalous sulfur isotope compositions of volcanic sulfate over the last millennium in Antarctic ice cores, J. Geophys. Res.-Atmos., 113, D20112, doi:10.1029/2008JD010185, 2008. 23981

Benson, D. R., Young, L. H., Kameel, F. R., and Lee, S. H.: Laboratory-measured nucleation rates of sulfuric acid and water binary homogeneous nucleation from the SO2 + OH reaction, Geophys. Res. Lett., 35, L11801, doi:10.1029/2008GL033387, 2008. 23961

Berresheim, H., Elste, T., Tremmel, H. G., Allen, A. G., Hansson, H. C., Rosman, K., Dal Maso, M., Makela, J. M., Kulmala, M., and O'Dowd, C. D.: Gas-aerosol relationships of H_2SO_4, MSA, and OH: Observations in the coastal marine boundary layer at Mace Head, Ireland, J. Geophys. Res.-Atmos., 107, 8100, doi:10.1029/2000JD000229, 2002. 23961

Bevington, P. and Robinson, D.: Data Reduction and Error Analysis for the Physical Sciences, Mc-Graw Hill, 23–28, 1992. 23969

Botha, C. F., Hahn, J., Pienaar, J. J., and Vaneldik, R.: Kinetics and mechanism of the oxidation of sulfur(IV) by ozone in aqueous solutions, Atmos. Environ., 28, 3207–3212, 1994. 23979

Bower, K. N. and Choularton, T. W.: Cloud processing of the Cloud Condensation Nucleus spectrum and its climatological consequences, Q. J. Roy. Meteorol. Soc., 119, 655–679, 1993. 23962

Cantrell, C. A., Zimmer, A., and Tyndall, G. S.: Absorption cross sections for water vapor from 183 to 193 nm, Geophys. Res. Lett., 24, 2195–2198, 1997. 23975

Title Page

Abstract | Introduction

Conclusions | References

Tables | Figures

|◄ | ►|

◄ | ►

Back | Close

Full Screen / Esc

Printer-friendly Version

Interactive Discussion

Caron, F., Tessier, A., Kramer, J. R., Schwarcz, H. P., and Rees, C. E.: Sulfur and oxygen isotopes of sulfate in precipitation and lakewater, Quebec, Canada, Appl. Geochem., 1, 601–606, 1986. 23964

Castleman, A. W., Munkelwitz, H. R., and Manowitz, B.: Isotopic Studies of Sulfur Component of Stratospheric Aerosol Layer, Tellus, 26, 222–234, 1974. 23981

Chin, M., Jacob, D. J., Gardner, G. M., ForemanFowler, M. S., Spiro, P. A., and Savoie, D. L.: A global three-dimensional model of tropospheric sulfate, J. Geophys. Res.-Atmos., 101, 18667–18690, 1996. 23961, 23962

Chmielewski, A. G., Derda, M., Wierzchnicki, R., and Mikolajczuk, A.: Sulfur isotope effects for the $SO_2(g)$-$SO_2(aq)$ system, Nukleonika, 47, S69–S70, 2002. 23978

Ding, T., Valkiers, S., Kipphardt, H., De Bievre, P., Taylor, P. D. P., Gonfiantini, R., and Krouse, R.: Calibrated sulfur isotope abundance ratios of three IAEA sulfur isotope reference materials and V-CDT with a reassessment of the atomic weight of sulfur, Geochimi. Cosmochim. Acta, 65, 2433–2437, 2001. 23963

Egiazarov, A. C., Kaviladze, M., Kerner, M. N., Oziashvili, E. L., Ebralidze, A., and Esakiya, A. D.: Separation of Sulfur Isotopes by Chemical Exchange, Isotopenpraxis: Isotopes in Environmental and Health Studies, 7, 379–383, 1971. 23964, 23973, 23979, 23982

Eriksen, T. E.: Sulfur Isotope Effects 1. Isotopic Exchange Coefficient for Sulfur Isotopes 34S-32S in System SO2(g)-HSO3(aq) at 25, 35, and 45 Degrees C, Acta Chemica Scandinavica, 26, 573, 1972a. 23961, 23964, 23973, 23979

Eriksen, T. E.: Sulfur Isotope Effects 2. Isotopic Exchange Coefficients for Sulfur Isotopes 34S-32S in System SO2(g)-Aqueous Solutions of SO_2, Acta Chem. Scand., 26, 581, 1972b. 23978, 23979

Eriksen, T. E.: Sulfur Isotope Effects 3. Enrichment of 34S by Chemical Exchange between SO2(g) and Aqueous Solutions of SO_2, Acta Chem. Scand., 26, 975, 1972c. 23979

Eriksen, T. E.: Sulfur Isotope Effects 4. Sulfur Isotope Effects in Anion-Exchange Systems, Acta Chemica Scandinavica, 26, 980, 1972d. 23979

Farquhar, J., Savarino, J., Airieau, S., and Thiemens, M. H.: Observation of wavelength-sensitive mass-independent sulfur isotope effects during SO2 photolysis: Implications for the early atmosphere, J. Geophys. Res.-Plan., 106, 32829–32839, 2001. 23976

Goldstein, D. E., N., Echlin, P., Joy, D., Fiori, C., and Lifshin, E.: Scanning Electron Microscopy and X-ray Microanalysis, Plenum Press, New York, USA, 1981. 23967

Groener, E. and Hoppe, P.: Automated ion imaging with the NanoSIMS ion microprobe, Appl.

Title Page

Abstract | Introduction

Conclusions | References

Tables | Figures

|◄ | ►|

◄ | ►

Back | Close

Full Screen / Esc

Printer-friendly Version

Interactive Discussion

Surf. Sci., 252, 7148–7151, doi:10.1016/j.apsusc.2006.02.280, 2006. 23968

Guo, Z. B., Li, Z. Q., Farquhar, J., Kaufman, A. J., Wu, N. P., Li, C., Dickerson, R. R., and Wang, P. C.: Identification of sources and formation processes of atmospheric sulfate by sulfur isotope and scanning electron microscope measurements, J. Geophys. Res.-Atmos., 115, D00K07, doi:10.1029/2009JD012893, 2010. 23964

Hanson, D. R. and Eisele, F.: Diffusion of H2SO4 in humidified nitrogen: Hydrated H_2SO_4, J. Phys. Chem. A, 104, 1715–1719, 2000. 23970

Herrmann, H., Ervens, B., Jacobi, H. W., Wolke, R., Nowacki, P., and Zellner, R.: CAPRAM2.3: A chemical aqueous phase radical mechanism for tropospheric chemistry, J. Atmos. Chem., 36, 231–284, 2000. 23961, 23974

Hoppe, P.: NanoSIMS: A new tool in cosmochemistry, Appl. Surf. Sci., 252, 7102–7106, 2006. 23968

Huygen, C.: The sampling of sulfur dioxide in air with impregnated filter paper, Anal. Chim. Acta, 28, 349–360, 1963. 23971

IPCC: Contribution of Working Group I to the Fourth Assessment Report of the Intergovernmental Panel on Climate Change, 2007, Cambridge University Press, http://www.ipcc.ch/publications_and_data/ar4/wg1/en/contents.html, 2007. 23962

Krouse, H. R. and Grinenko, V. A.: Stable isotopes : natural and anthropogenic sulphur in the environment, vol. 43, Wiley, Chichester, UK, 1991. 23963

Kulmala, M., Vehkamaki, H., Petaja, T., Maso, M. D., Lauri, A., Kerminen, V. M., Birmili, W., and McMurry, P. H.: Formation and growth rates of ultrafine atmospheric particles: a review of observations, J. Aerosol Sci., 35, 143–176, 2004. 23961

Lai, A. C.: Investigation of Electrostatic Forces on Particle Deposition in a Test Chamber, Indoor Built Environ., 15, 179–186, 2006. 23970

Leung, F. Y., Colussi, A. J., and Hoffmann, M. R.: Sulfur isotopic fractionation in the gas-phase oxidation of sulfur dioxide initiated by hydroxyl radicals, J. Phys. Chem. A, 105, 8073–8076, 2001. 23964, 23980, 23981

Luz, B. and Barkan, E.: The isotopic ratios O-17/O-16 and O-18/O-16 in molecular oxygen and their significance in biogeochemistry, Geochim. Cosmochim. Acta, 69, 1099–1110, 2005. 23981

Lyons, J. R.: Atmospherically-derived mass-independent sulfur isotope signatures, and incorporation into sediments, Chem. Geol., 267, 164–174, 2009. 23976

Mariotti, A., Germon, J. C., Hubert, P., Kaiser, P., Letolle, R., Tardieux, A., and Tardieux, P.:

Experimental-determination of Nitrogen Kinetic Isotope Fractionation - Some Principles – Illustration For the Denitrification and Nitrification Processes, Plant Soil, 62, 413–430, 1981. 23963, 23972

Mertes, S., Lehmann, K., Nowak, A., Massling, A., and Wiedensohler, A.: Link between aerosol hygroscopic growth and droplet activation observed for hill-capped clouds at connected flow conditions during FEBUKO, Atmos. Environ., 39, 4247–4256, 2005. 23962

Moore, J., Stanitski, C., and Jurs, P.: Chemistry: The Molecular Science, Brooks/Cole – Thomson Learning, USA, 2005. 23962

Mukai, H., Tanaka, A., Fujii, T., Zeng, Y. Q., Hong, Y. T., Tang, J., Guo, S., Xue, H. S., Sun, Z. L., Zhou, J. T., Xue, D. M., Zhao, J., Zhai, G. H., Gu, J. L., and Zhai, P. Y.: Regional characteristics of sulfur and lead isotope ratios in the atmosphere at several Chinese urban sites, Environ. Sci. Technol., 35, 1064–1071, 2001. 23980

Norman, A. L., Anlauf, K., Hayden, K., Thompson, B., Brook, J. R., Li, S. M., and Bottenheim, J.: Aerosol sulphate and its oxidation on the Pacific NW coast: S and O isotopes in $PM_{2.5}$, Atmos. Environ., 40, 2676–2689, 2006. 23964, 23980

Novak, M., Bottrell, S. H., and Prechova, E.: Sulfur isotope inventories of atmospheric deposition, spruce forest floor and living Sphagnum along a NW-SE transect across Europe, Biogeochemistry, 53, 23–50, 2001a. 23963, 23964, 23971

Novak, M., Jackova, I., and Prechova, E.: Temporal Trends in the Isotope Signature of Air-Borne Sulfur in Central Europe, Environ. Sci. Technol., 35, 255–260, 2001b. 23980

Nriagu, J. O., Rees, C., Mekhtiyeva, V., Lein, A., Fritz, P., Drimmie, R., Pankina, R., Robinson, B., and Krouse, H. R.: Stable Isotopes: Natural and Anthropogenic Sulphur in the Environment, chap. 6., John Wiley and Sons, 177–266, 1991. 23972

Ohizumi, T., Fukuzaki, N., and Kusakabe, M.: Sulfur isotopic view on the sources of sulfur in atmospheric fallout along the coast of the Sea of Japan, Atmos. Environ., 31, 1339–1348, 1997. 23964

Ono, S., Wing, B., Johnston, D., Farquhar, J., and Rumble, D.: Mass-dependent fractionation of quadruple stable sulfur isotope system as a new tracer of sulfur biogeochemical cycles, Geochim. Cosmochim. Acta, 70, 2238–2252, 2006a. 23972, 23990

Ono, S., Wing, B., Rumble, D., and Farquhar, J.: High precision analysis of all four stable isotopes of sulfur (S-32, S-33, S-34 and S-36) at nanomole levels using a laser fluorination isotope-ratio-monitoring gas chromatography-mass spectrometry, Chem. Geol., 225, 30–39, 2006b. 23996

Sulfur isotope fractionation during oxidation of sulfur dioxide

E. Harris et al.

Title Page

Abstract	Introduction
Conclusions	References
Tables	Figures

|◄ | ►|

◄ | ►

Back | Close

Full Screen / Esc

Printer-friendly Version

Interactive Discussion

Patris, N., Delmas, R. J., and Jouzel, J.: Isotopic signatures of sulfur in shallow Antarctic ice cores, J. Geophys. Res.-Atmos., 105, 7071–7078, 2000. 23963

Rees, C. and Holt, B.: Stable Isotopes: Natural and Anthropogenic Sulphur in the Environment, chap. 3., John Wiley and Sons, 43–64, 1991. 23965

Rees, C. E., Jenkins, W. J., and Monster, J.: Sulfur Isotopic Composition of Ocean Water Sulfate, Geochim. Cosmochim. Acta, 42, 377–381, 1978. 23963

Saltzman, E. S., Brass, G., and Price, D.: The mechanism of sulfate aerosol formation: Chemical and sulfur isotopic evidence, Geophys. Res. Lett., 10, 513–516, 1983. 23964, 23978, 23980

Savarino, J., Lee, C. C. W., and Thiemens, M. H.: Laboratory oxygen isotopic study of sulfur (IV) oxidation: Origin of the mass-independent oxygen isotopic anomaly in atmospheric sulfates and sulfate mineral deposits on Earth, J. Geophys. Res.-Atmos., 105, 29079–29088, 2000. 23981

Seinfeld, J. H. and Pandis, S. N.: Atmospheric Chemistry and Physics, Wiley & Sons, New York, USA, 1203, 1998. 23961, 23962, 23974

Sinha, B. W., Hoppe, P., Huth, J., Foley, S., and Andreae, M. O.: Sulfur isotope analyses of individual aerosol particles in the urban aerosol at a central European site (Mainz, Germany), Atmos. Chem. Phys., 8, 7217–7238, doi:10.5194/acp-8-7217-2008, 2008a. 23964, 23980

Sinha, V., Williams, J., Crowley, J. N., and Lelieveld, J.: The Comparative Reactivity Method – a new tool to measure total OH Reactivity in ambient air, Atmos. Chem. Phys., 8, 2213–2227, doi:10.5194/acp-8-2213-2008, 2008b. 23975

Sinha, V., Custer, T. G., Kluepfel, T., and Williams, J.: The effect of relative humidity on the detection of pyrrole by PTR-MS for OH reactivity measurements, Int. J. Mass Spectrom., 282, 108–111, 2009. 23975

Slodzian, G., Chaintreau, M., Dennebouy, R., and Rousse, A.: Precise in situ measurements of isotopic abundances with pulse counting of sputtered ions, Europ. Phys. J.-Appl. Phys., 14, 199–231, 2001. 23969

Slodzian, G., Hillion, F., Stadermann, F. J., and Zinner, E.: QSA influences on isotopic ratio measurements, Appl. Surf. Sci., 231-2, 874–877, 2004. 23969

Sofen, E. D., Alexander, B., and Kunasek, S. A.: The impact of anthropogenic emissions on atmospheric sulfate production pathways, oxidants, and ice core $\Delta^{17}O(SO_4^2)$, Atmos. Chem. Phys., 11, 3565-3578, doi:10.5194/acp-11-3565-2011, 2011. 23981

Stoyan, D.: Stochastik fuer Ingenieure und Naturwissenschaftler, Wiley-VCH, 1998. 23968

Sulfur isotope fractionation during oxidation of sulfur dioxide

E. Harris et al.

Title Page

Abstract | Introduction

Conclusions | References

Tables | Figures

◄ | ►

◄ | ►

Back | Close

Full Screen / Esc

Printer-friendly Version

Interactive Discussion

Tanaka, N., Rye, D. M., Xiao, Y., and Lasaga, A. C.: Use of Stable Sulfur Isotope Systematics for Evaluating Oxidation Reaction Pathways and in-Cloud Scavenging of Sulfur-Dioxide in the Atmosphere, Geophys. Res. Lett., 21, 1519–1522, 1994. 23961, 23964, 23980

US-EPA: Method 6 – Determination of Sulfur Dioxide Emissions from Stationary Sources, http://www.epa.gov/ttn/emc/, 2010. 23972

Winterholler, B.: Sulfur Isotope Analysis of Aerosol Particles by NanoSIMS, Ph.D. thesis, Johannes Gutenberg-Universitaet, Mainz, Germany, 2007. 23967, 23968

Winterholler, B., Hoppe, P., Andreae, M. O., and Foley, S.: Measurement of sulfur isotope ratios in micrometer-sized samples by NanoSIMS, Appl. Surf. Sci., 252, 7128–7131, 2006. 23968

Winterholler, B., Hoppe, P., Foley, S., and Andreae, M. O.: Sulfur isotope ratio measurements of individual sulfate particles by NanoSIMS, Int. J. Mass Spectrom., 272, 63–77, 2008. 23968

Young, L. H., Benson, D. R., Kameel, F. R., Pierce, J. R., Junninen, H., Kulmala, M., and Lee, S.-H.: Laboratory studies of H_2SO_4/H_2O binary homogeneous nucleation from the SO_2+OH reaction: evaluation of the experimental setup and preliminary results, Atmos. Chem. Phys., 8, 4997–5016, doi:10.5194/acp-8-4997-2008, 2008. 23970, 23975

Zasypkin, A., Grigor'eva, V., Korchak, V., and Gerschenson, Y.: A formula for summing of kinetic resistances for mobile and stationary media: I. Cylindrical reactor, Kin. Catalys., 38, 842–851, 1997. 23970

Table 1. Fractionation of $^{34}S/^{32}S$ and $^{33}S/^{32}S$ between two collectors in series during collection of H_2SO_4.

Run #	1	2	3	Average
Date	02.11.09	03.11.09	23.02.10	
N_2 flow rate (sccm)	1500	1500	1720	
Length (h)	6.3	8.3	6.1	
$\delta^{34}S_{C_1} - \delta^{34}S_{C_2}$	−3.3±2.1	2.4±2.5	−4.2±7.9	**−1.1±2.6**
$\delta^{33}S_{C_1} - \delta^{33}S_{C_2}$	0.7±2.2	−0.4±2.3	0.9±3.6	**0.3±1.5**

Table 2. Fractionation of $^{34}S/^{32}S$ during collection of SO_2 in a solution of H_2O_2. [1] Measured by traditional duel-inlet isotope ratio mass spectrometry (Ono et al., 2006a) by Shuhei Ono (2010). [2] All values are corrected for the initial isotopic composition of +1.25 ‰. [3] Found from $\delta^{34}S_{tot} = \left(\delta^{34}S_{P_1} + f \cdot \delta^{34}S_{P_2} \right) / (1 + f)$ for samples where the bubblers were measured separately.

Run #	1	2	3	4	5	6	7	8[1]	Average
Date	30.10.09	05.11.09	10.11.09	19.02.10	22.02.10	31.03.10	21.04.10	19.07.10	
Length (h)	6.0	6.6	5.6	3.0	2.9	4.1	5.6	3.2	
H_2O_2 volume (mL)	180	180	180	300	300	300	300	300	
$[H_2O_2]$ (%)	5	5	6	5	5	6	6	6	
$[SO_2]$ (ppm)	7.6	7.6	7.6	0.35	0.35	0.13	0.39	2.0	
SO_2 flow rate (sccm)	1022	1022	1022	1700	1700	1700	600	510	
Gas Temperature	Room T	Room T	Room T	Room T	Room T	40 °C	Room T	Room T	
f	0.57	0.83		0.58	0.61	0.66			0.61±0.11
$\delta^{34}S$, 1st bubbler[2]	14.3±2.1	9.6±3.5	8.7±7.8	12.5±1.5	11.4±2.4	11.5±1.3			11.1±0.8
$\delta^{34}S$, 2nd bubbler[2]	3.2±1.8	8.9±3.5		3.2±0.9	4.3±5.5	5.4±2.2			3.7± 0.7
$\delta^{34}S$, product[3]	10.1±2.8	9.3±4.9	6.6±7.9	9.1±1.7	8.7±6.0	9.2±2.5	11.1±3.2	9.1±1.0	9.2± 0.7
α	1.017	1.016	1.011	1.015	1.015	1.015	1.019	1.016	1.016±0.001

E. Harris et al.

Table 3. Fractionation factors at 19 °C for the aqueous oxidation of SO_2 by radical chain reaction initiated by Fe, H_2O_2 bulk solution (from temperature-dependent regression), and H_2O_2/O_3 and only O_3 in aerosol droplets.

Oxidant	α_{34}	$1\,\sigma$	α_{33}	$1\,\sigma$
H_2O_2	1.015	0.0013	1.007	0.0016
O_3	1.017	0.0028	1.016	0.0022
H_2O_2/O_3	1.009	0.0062	1.006	0.0012
radical chain	0.989	0.0043	0.993	0.0022

Table 4. Temperature dependent fractionation factors during the gas-phase oxidation of SO_2 by OH radicals.

T (°C)	n	α_{34}	1 σ	α_{33}	1 σ
−20	2	1.0095	0.0013	1.0034	0.0014
2	3	1.0088	0.0030	1.0053	0.0012
19	4	1.0113	0.0024	1.0053	0.0049
38	3	1.0052	0.0028	1.0034	0.0009
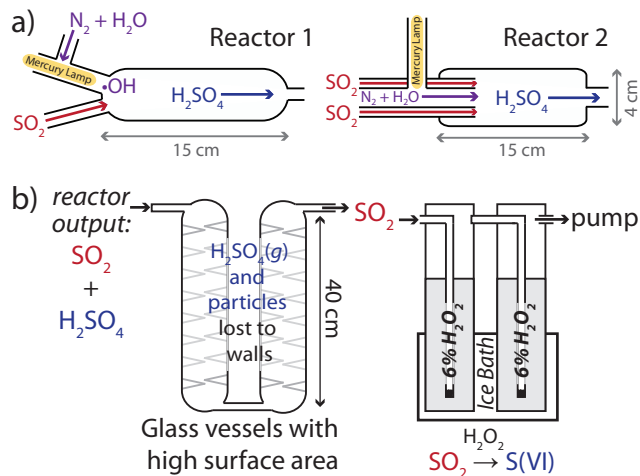
Fig. 1. Reaction system used to investigate oxidation of SO$_2$: **(a)** reactors, **(b)** collection system.
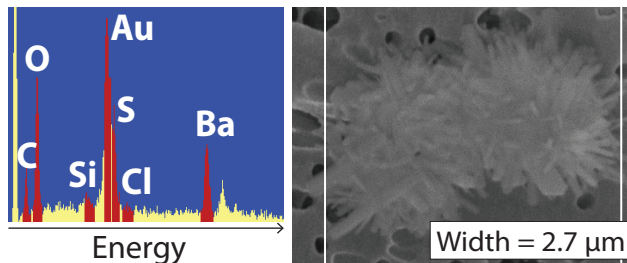
Fig. 2. EDX spectrum and SEM image of a typical BaSO$_4$ grain.
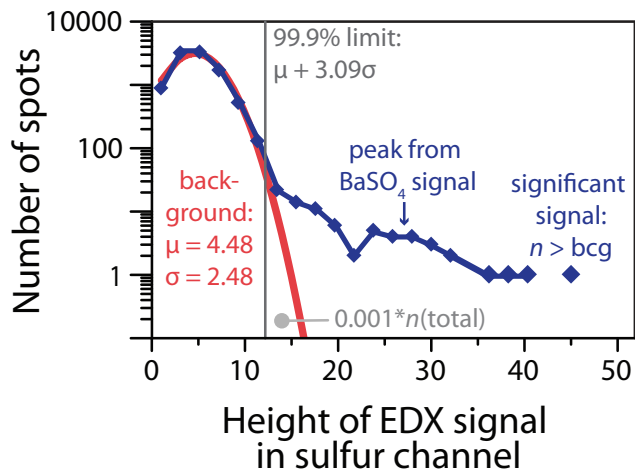
Fig. 3. Frequency of signal height in the sulfur channel of an automatic EDX analysis of $BaSO_4$ on a gold-coated filter. The measured signal for the sulfur channel is shown in blue and the Gaussian fit to the contribution from the gold peak is shown in red.
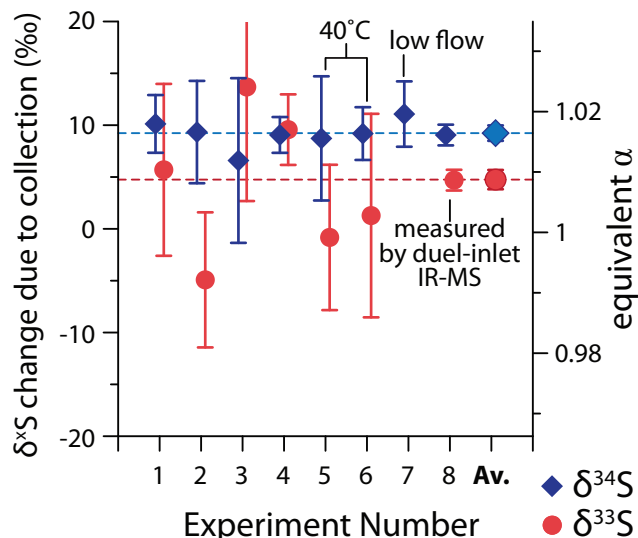
Fig. 4. Fractionation introduced during collection of SO_2 in H_2O_2 solution. The laser fluorination sample was measured as described in Ono et al. (2006b). The shown data of experiments 1–7 are the weighted averages of individual NanoSIMS measurements, while the horizontal dashed lines and the two data points at the right side show the weighted averages of all experiments.
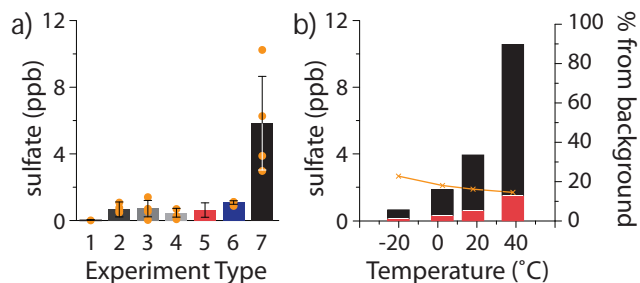
Fig. 5. Quantification of background in the reaction of SO_2 and OH. **(a)** Total sulfate collected at room temperature under various conditions (individual samples are shown as orange dots, error bars are 1σ standard deviation of individual samples): (1) Background from impurities in MilliQ water and $BaCl_2$; (2) Direct photolysis of SO_2, 254 nm and 185 nm lines; (3) Direct photolysis, 254 nm line; (4) 254 nm and 185 nm lines, humidity passing over lamp; (5) 2–4 combined to show total production under UV light in the absence of OH; (6) no irradiation, no added oxidant; 7) 11 ppb OH. **(b)** Temperature-dependence of sulfate production from OH reaction (black) and background from sulfate impurities in water (white) and background production (red), with the percentage contribution of the background to total collected shown in orange.
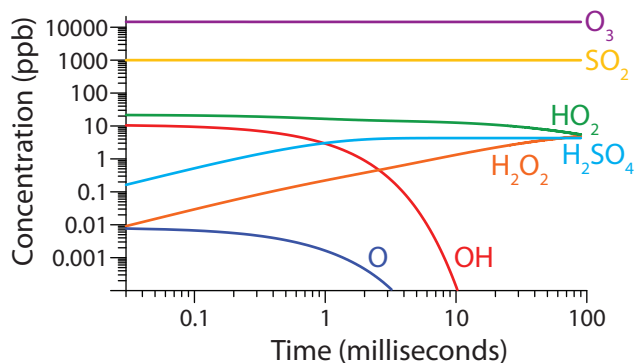
Fig. 6. Facsimile model of potential oxidants and H_2SO_4 produced as 11 ppb OH is generated from the photolysis of water in 20 % oxygen and mixed with 1 ppm SO_2 at atmospheric pressure.

Title Page

Abstract | Introduction

Conclusions | References

Tables | Figures

◄ | ►I

◄ | ►

Back | Close

Full Screen / Esc

Printer-friendly Version

Interactive Discussion
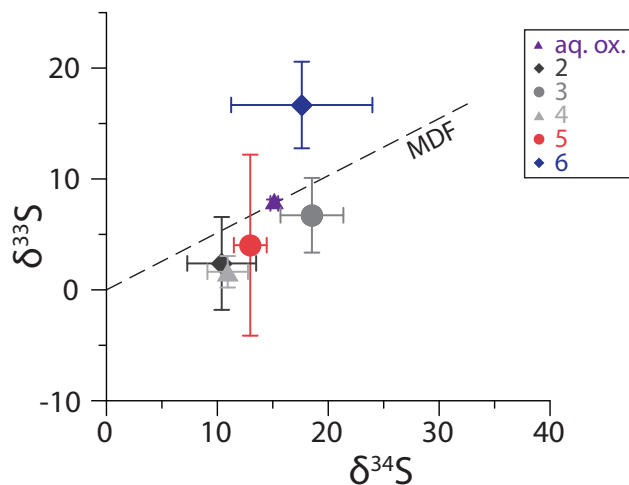
Fig. 7. Isotopic composition of interferences in the reaction of SO_2 and OH. See Fig. 5 for explanation of legend numbers. Aq. ox. shows the isotopic composition of the products of aqueous oxidation by H_2O_2 or O_3.

Fig. 8. Fractionation factors at 19 °C for the aqueous oxidation of SO_2 by radical chain reaction initiated by Fe, H_2O_2 bulk solution (from temperature-dependent regression), and H_2O_2/O_3 and only O_3 in aerosol droplets.

Fig. 9. Temperature dependence of fractionation during aqueous oxidation of SO_2 by H_2O_2 and O_3.
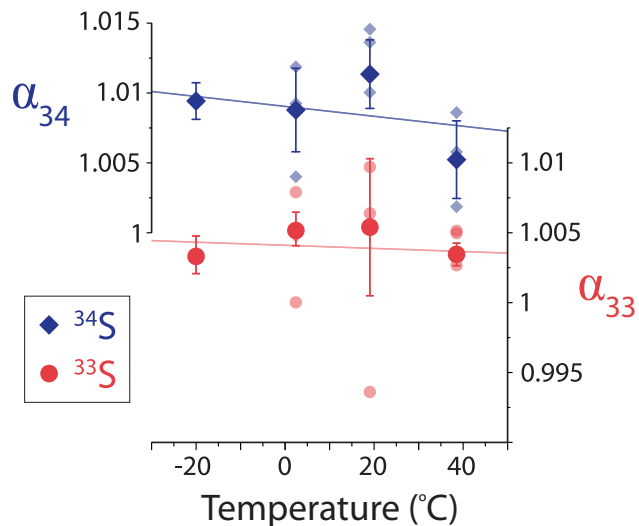
Fig. 10. Temperature dependent fractionation factors during the gas-phase oxidation of SO_2 by OH radicals. Pale points represent individual experiments while dark points with error bars are the average and 1σ error of the mean at each temperature.